High-Speed Humanoid Running Through Control with a 3D-SLIP Model

Patrick M. Wensing and David E. Orin

***Abstract*— This paper presents new methods to control high-speed running in a simulated humanoid robot at speeds of up to 6.5 m/s. We present methods to generate compliant target CoM dynamics through the use of a 3D spring-loaded inverted pendulum (SLIP) template model. A nonlinear least-squares optimizer is used to find periodic trajectories of the 3D-SLIP offline, while a local deadbeat SLIP controller provides reference CoM dynamics online at real-time rates to correct for tracking errors and disturbances. The local deadbeat controller employs common foot placement strategies that are automatically generated by a local analysis of the 3D-SLIP apex return map. A task-space controller is then applied online to select whole-body joint torques which embed these target dynamics into the humanoid. Despite the body of work on the 2D and 3D-SLIP models, to the best of the authors' knowledge, this is the first time that a SLIP model has been embedded into a whole-body humanoid model. When running at 3.5 m/s, the controller is shown to reject lateral disturbances of 40 N·s applied at the waist. A final demonstration shows the capability of the controller to stabilize running at 6.5 m/s, which is comparable with the speed of an Olympian in the 5000 meter run.**

I. Introduction

The Spring-Loaded Inverted Pendulum (SLIP) model has been shown to describe the center of mass (CoM) dynamics remarkably well for high-speed locomotion in a variety of insects and animals [1]. Despite its simplicity, whether hopping, trotting, or running, creatures from cockroaches to kangaroos bounce dynamically, in close accordance with the SLIP model [1]. As opposed to low-speed locomotion, where animals typically vault over stiff legs, high-speed gaits employ compliant CoM dynamics. In biological systems, this compliance is shown to play a role in adapting to varied terrain [2], and enables a reduced metabolic cost over stiff gaits at high-speeds [3].

These advantages, afforded by elasticity found in biological muscles and tendons, have inspired increased interest to develop high-performance compliant actuators [4]. Despite these advances, control of humanoid running remains a sparsely studied problem, with solution methods largely adapted from inverted pendulum methods for walking [5], [6]. Other methods have required intensive hand design [7] or offline optimization [8] and have not shown robustness to disturbances. In contrast to these methods, this paper develops control approaches for high-speed running in a humanoid based on a 3D-SLIP model. To the best of the authors' knowledge, this represents the first time that a SLIP model has been used to generate whole-body humanoid motion. By matching the CoM dynamics of a humanoid model, shown in Fig. 1, to a 3D-SLIP model, the control approach described here is able to demonstrate running in simulation at speeds from 3.5-6.5 m/s, is able to reject push disturbances, and to change speeds in a single step.

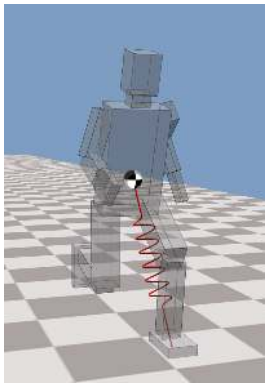

Fig. 1. High-speed humanoid running is demonstrated in simulation by commanding the Center of Mass (CoM) dynamics of the humanoid to match that of a 3D-SLIP model. The red spring in this figure represents the compliant target CoM behavior. The humanoid employs torque control at its joints to embed the 3D-SLIP dynamics.

Two-dimensional SLIP models have been quite useful in the control and analysis of hopping monopods and bipeds in the sagittal plane. Poulakakis and Grizzle formally embed an extension of the 2D-SLIP model into the dynamics of a hopping monopod [9] with a geometric nonlinear control approach. Hutter et al. [10] studied a SLIP model with an operational-space controller for CoM tracking to regulate hop height and velocity in a simulated leg. Rutschmann et al. [11] applied nonlinear model predictive control to plan SLIP trajectories for uneven terrain footholds. Garofalo et al. [12] developed a 2D-walking controller based on a bipedal SLIP model. While humanoid running is largely dominated by sagittal plane dynamics, these controllers do not have the generality to control lateral sway in humanoid running, and do not provide insight into lateral footstep selection for disturbances. These cases are automatically handled here.

Three-dimensional SLIP models have recently been proposed as a generalization of planar SLIP models. While these 3D-SLIP models have been the subject of analytical studies [13], [14], their application to trajectory generation and control of humanoid robots has yet to emerge. Seipel and Holmes develop approximations to the 3D-SLIP step-to-

P. M. Wensing is a PhD student in the Department of Electrical and Computer Engineering, The Ohio State University: wensing.2@osu.edu

D. E. Orin is a Professor Emeritus in the Department of Electrical and Computer Engineering, The Ohio State University: orin.1@osu.edu

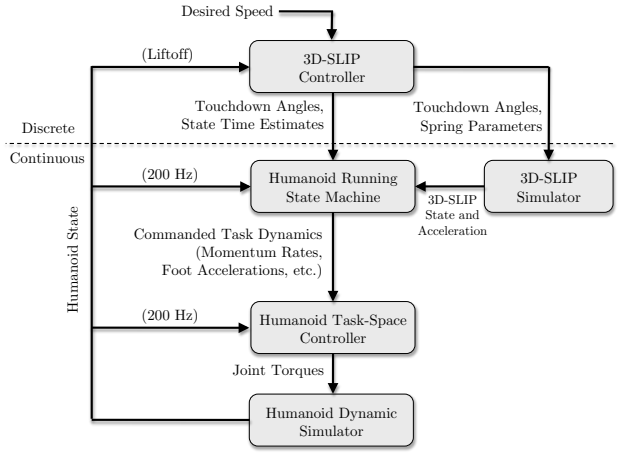

Fig. 2. Block diagram of the control system. Once per step (at each liftoff) a 3D-SLIP controller selects touchdown angles and target CoM compliance characteristics to achieve a desired speed by the end of the next step. A humanoid state machine then selects appropriate task dynamics for the foot and CoM to continuously track the SLIP CoM dynamics and realize the desired foot touchdown locations. The state machine also selects desired angular momentum rates in stance to promote balance. A Humanoid Task-Space Controller then selects whole-body joint torques at real-time rates to realize these desired tasks.

step dynamics and show the inherent instability of periodic 3D-SLIP gaits [13]. Carver [14] treats the 3D-SLIP model as a monopod in 3D and analyzes a number of control problems for 3D steering. While modifications are required for application to humanoids, the work in [14] serves as inspiration for the 3D-SLIP control presented here.

The block diagram of the control system used in this paper is shown in Fig. 2. The control includes a discrete component that selects touchdown angles at each liftoff and provides target CoM dynamics based on the 3D-SLIP after the next foot touchdown. A continuous component, provided by a state machine and task-space controller, is then capable to reproduce these target dynamics through torque control of the humanoid robot.

The remainder of the paper is organized as follows. Section II presents the 3D-SLIP model and its associated control system. A new method is presented which produces periodic 3D-SLIP trajectories that are able to be retargeted to the humanoid. Periodic trajectories are found through formulation of a nonlinear least-squares optimization problem and natural gait timings are specified from biomechanics data. A local deadbeat control approach is introduced to stabilize these trajectories. The controller is specified automatically, without required tuning, from a local analysis of 3D-SLIP step-to-step dynamics. Section III presents methods to track these target CoM dynamics with a Task-Space Control approach similar to [15]. As a key feature, the controller applies angular momentum control which enables upper body motions that reduce the required yaw moment for the motion. Section IV presents running results for single-speed running, speed transitions, and disturbance recovery. A top speed of 6.5 m/s is able to be controlled by the approach presented. Section V ends with conclusions and suggestions for further study. A video of the running results is provided in an attachment to this paper.

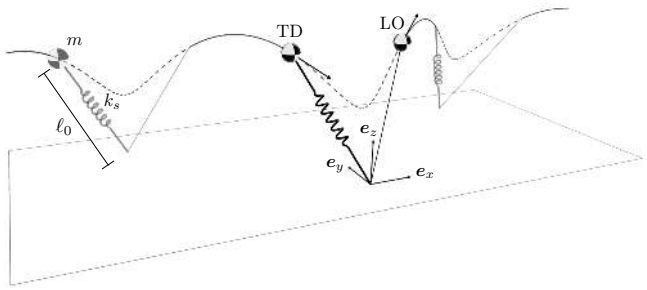

Fig. 3. 3D-SLIP template model for high-speed humanoid running. The 3D-SLIP is a nominally passive point-mass model of locomotion.

II. 3D-SLIP Model and Control

A. The 3D Spring-Loaded Inverted Pendulum Model

Planar spring-mass models of locomotion have been extensively studied in recent decades to describe the center-of-mass (CoM) dynamics of a wide range of animals [1]. The 3D spring-loaded inverted pendulum (3D-SLIP) model, shown in Fig. 3, is a natural generalization of the common planar SLIP model, and is capable to describe a richer set of CoM dynamics [13]. The model consists of a point-mass m and leg that experiences phases of stance and flight. The mass follows ballistic dynamics in flight wherein the massless leg is positioned for upcoming stance. Following touchdown (TD), a Hookean spring with constant k_s and rest length ℓ_0 imparts forces onto the mass. The period of stance ends at liftoff (LO) when the spring once again reaches its rest length. It is assumed that forward motion is in the positive x-direction throughout, as shown in Fig. 3.

The evolution of the 3D-SLIP model can be described more precisely as a hybrid dynamic system. We assume the position of the mass to be given in inertial coordinates as $\boldsymbol{p}_s \in \mathbb{R}^3$ with velocity $\dot{\boldsymbol{p}}_s \in \mathbb{R}^3$. Flight dynamics follow $m\,\ddot{\boldsymbol{p}}_s = m\,\boldsymbol{g}$, where $\boldsymbol{g} \in \mathbb{R}^3$ is the gravity vector. In flight, the foot position $\boldsymbol{p}_f \in \mathbb{R}^3$ is adjusted for the upcoming stance with touchdown angles θ and $\boldsymbol{\phi}$, shown in Fig. 4, as

$$\boldsymbol{p}_f = \boldsymbol{p}_s + \boldsymbol{p}_{hip} + \ell_h \begin{bmatrix} \sin(\theta)\cos(\phi) \\ -\sin(\theta)\sin(\phi) \\ -\cos(\theta) \end{bmatrix} . \qquad (1)$$

Here ℓ_h represents the length of the humanoid virtual leg (hip to foot center) at touchdown, and $\boldsymbol{p}_{hip}$ is the position of the hip with respect to the CoM. As an alternative to using touchdown angles θ and ϕ to specify the SLIP anchor relative to the CoM, a hip offset is applied so that these touchdown angles more closely correspond to angles of the humanoid virtual leg. This is a modification over previous work [13], [14] that enables more direct application of the 3D-SLIP template to the humanoid. Here it is assumed that the hip is offset from the CoM laterally by amount y_{hip} which nominally equals half the width of the torso.

In stance, the dynamics follow

$$m\,\ddot{\boldsymbol{p}}_s = k_s(\ell_0 - ||\boldsymbol{\ell}||)\,\hat{\boldsymbol{\ell}} + m\,\boldsymbol{g} \qquad (2)$$

where ℓ_0 is the rest length of the spring (computed as its length at touchdown) and $\boldsymbol{\ell} \in \mathbb{R}^3$ is given by $\boldsymbol{\ell} = \boldsymbol{p}_s - \boldsymbol{p}_f$.

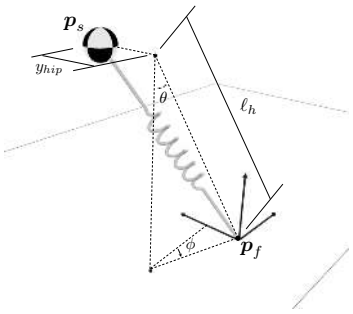

Fig. 4. Touchdown angle definitions. Hip displacement is shown for a right foot touchdown.

Transitions to and from stance occur when the 3D-SLIP state intersects the TD and LO switching manifolds respectively:

$$\mathcal{S}_{TD} = \{(\boldsymbol{p}_s, \dot{\boldsymbol{p}}_s) \mid \boldsymbol{e}_z^T \boldsymbol{p}_s = \ell_h \cos(\theta),\, \boldsymbol{e}_z^T \dot{\boldsymbol{p}}_s \leq 0\}, \quad (3)$$

$$\mathcal{S}_{LO} = \left\{(\boldsymbol{p}_s, \dot{\boldsymbol{p}}_s) \mid ||\boldsymbol{\ell}|| = \ell_0,\, \boldsymbol{\ell}^T \dot{\boldsymbol{p}}_s \geq 0\right\} . \quad (4)$$

B. 3D-SLIP Apex Return Map

We are interested in controlling the 3D-SLIP model from step-to-step by varying its touchdown angles and spring characteristics. As one of several approaches, this paper concentrates on control of the top-of-flight (TOF) height and velocity. An apex state-of-interest $\mathbf{x}$ is thus constructed from the full SLIP state $(\boldsymbol{p}_s, \dot{\boldsymbol{p}}_s)$ by:

$$\mathbf{x} = \begin{bmatrix} \boldsymbol{e}_z^T \boldsymbol{p}_s \\ \boldsymbol{e}_x^T \dot{\boldsymbol{p}}_s \\ \boldsymbol{e}_y^T \dot{\boldsymbol{p}}_s \end{bmatrix} = \begin{bmatrix} h \\ v_x \\ v_y \end{bmatrix} \quad (5)$$

where $\boldsymbol{e}_x$, $\boldsymbol{e}_y$, and $\boldsymbol{e}_z$ are the unit vectors shown in Fig. 3. Given touchdown angles and spring characteristics described by $\mathbf{u}_n$ for the n-th step, an apex return map can be formed:

$$\mathbf{x}_{n+1} = \boldsymbol{f}(\mathbf{x}_n, \mathbf{u}_n) \quad (6)$$

which maps the TOF state $\mathbf{x}_n$ to the subsequent TOF state. Since the 3D-SLIP is a passive model, active additions need to be considered to enable the 3D-SLIP to change speeds or to recover from disturbances. Here, it is assumed that the spring stiffness k_s can vary at the instant of maximum spring compression. Denoting these control variables before and after maximum compression as k_{s_1} and k_{s_2}, the control decisions $\mathbf{u}$ for each step are collected as

$$\mathbf{u} = [\theta,\, \phi,\, k_{s_1},\, k_{s_2}]^T . \quad (7)$$

Given a desired forward speed, Section II-C introduces a method to find an initial apex state $\mathbf{x}_0$ and control $\mathbf{u}_0$ that will lead to periodic 3D-SLIP dynamics. Since it is of interest to find 2-step periodic motions of the 3D-SLIP, search for 1-step motions is restricted to those with alternating lateral velocity, but constant height and forward velocity at each TOF. One-step motions are thus desired with

$$\boldsymbol{A}\,\mathbf{x}_0 = \boldsymbol{f}(\mathbf{x}_0, \mathbf{u}_0) . \quad (8)$$

where $\boldsymbol{A} = \mathrm{diag}(1, 1, -1)$. Section II-D then presents a method to stabilize these periodic trajectories by developing 3D-SLIP controllers for different speeds.

C. Finding Periodic 3D-SLIP Trajectories

For any given forward speed, the 3D-SLIP model exhibits an infinite number of periodic trajectories. For instance, by adjusting touchdown angles and leg stiffnesses, periodic gaits can be generated with different maximum heights, or different lateral sway characteristics. A method is introduced here which uses offline optimization to find periodic 3D-SLIP trajectories that approximately mimic human locomotion and are able to be retargeted to the humanoid model.

Human running data in [16] and [17] is used to specify target gait timings of the 3D-SLIP model. Studies have shown that human cadence c (steps per minute) increases [16] and stance time t_s decreases [17] with increased speed. Based on the data in these studies, the following relationships were determined:

$$c = 2.55 v_x^2 - 8.77 v_x + 172.9 \quad (9)$$

$$\log_{10}(t_s) = -0.64 \log_{10}(v_x) - 0.2 . \quad (10)$$

To provide additional time for leg positioning in flight, cadence was unmodified while target stance times were shortened to be governed by the following equation:

$$t_s = 10^{-0.2}\, v_x^{-0.82} . \quad (11)$$

These relationships can be used to determine desired TD and LO times $\boldsymbol{T}_d(v_x) = [t_{TD,d},\, t_{LO,d}]^T$ as a function of forward velocity. Given a TOF-state and control pair, dynamic simulation can be used to evaluate the actual TD and LO times. This evaluation is denoted by the mapping $\boldsymbol{g}$:

$$[t_{TD},\, t_{LO}]^T = \boldsymbol{g}(\mathbf{x}_n, \mathbf{u}_n) . \quad (12)$$

Given a desired forward TOF velocity v_x, a least-squares optimization problem can then be formulated to find a state-control pair which matches the periodicity constraint (8) and achieves the desired gait timings:

$$\min_{h_0, v_{y0}, k_s, \theta} \; ||\boldsymbol{A}\,\mathbf{x}_0 - \boldsymbol{f}(\mathbf{x}_0, \mathbf{u}_0)||^2 + ||\boldsymbol{T}_d(v_x) - \boldsymbol{g}(\mathbf{x}_0, \mathbf{u}_0)||^2 \quad (13)$$

$$\text{where } \mathbf{x}_0 = [h_0,\, v_x,\, v_{y0}]^T \quad (14)$$

$$\mathbf{u}_0 = [\theta,\, 0,\, k_s,\, k_s]^T . \quad (15)$$

Note that a touchdown angle of $\phi = 0$ has been fixed to ensure a gait with footstep locations directly in front of the hips. Additionally, the spring stiffnesses k_{s_1} and k_{s_2} are selected to be equal, since any change in stiffness would change the 3D-SLIP total energy and prevent satisfaction of (8). This optimization, was performed in MATLAB with the nonlinear least-squares function `lsqnonlin`. Despite the need to use dynamic simulation in the evaluation of $\boldsymbol{f}$ and $\boldsymbol{g}$, the optimization is solved quickly in MATLAB. For instance, it takes approximately 20 seconds to generate 31 periodic 3D-SLIP gaits for forward speeds of 3.5 m/s to 6.5 m/s (at 0.1 m/s increments). Over this range of speeds, the optimal state-control pairs $(\mathbf{x}_0^*, \mathbf{u}_0^*)$ exhibit velocity-dependent touchdown angles and leg stiffnesses which increase with speed from 23.1 to 26.5 degrees and 11.7 to

16.4 kN/m respectively. The optimized TOF heights decrease only slightly with speed, from 91.0 cm at 3.5 m/s to 88.0 cm at 6.5 m/s.

D. 3D-SLIP Control - Transitioning to Periodic Motion

Once periodic 3D-SLIP motions have been generated, a 3D-SLIP controller is desired to transition from nearby TOF states to a periodic trajectory. Deadbeat control laws can be developed to achieve this goal in a single step but often require online optimization [10] or large knowledge bases [14]. Here a first-order approximation to a deadbeat controller is developed around the periodic apex state. The control law is easy to compute offline and can be applied online for real-time control of a humanoid.

Let $(\mathbf{x}_0^*, \mathbf{u}_0^*)$ be a state-control pair which satisfies (8) as computed in the previous section. A first order approximation to the return map around $(\mathbf{x}_0^*, \mathbf{u}_0^*)$ provides:

$$\mathbf{x}_1 = \boldsymbol{f}(\mathbf{x}_0^* + \Delta\mathbf{x}, \mathbf{u}_0^* + \Delta\mathbf{u}) \tag{16}$$

$$\approx \boldsymbol{A}\,\mathbf{x}_0^* + \boldsymbol{J}_x\,\Delta\mathbf{x} + \boldsymbol{J}_u\,\Delta\mathbf{u} \tag{17}$$

where $\boldsymbol{J}_x = \partial\boldsymbol{f}/\partial\mathbf{x}$ and $\boldsymbol{J}_u = \partial\boldsymbol{f}/\partial\mathbf{u}$ are Jacobians of the return map evaluated at $(\mathbf{x}_0^*, \mathbf{u}_0^*)$. These Jacobians can be evaluated numerically with finite differences. For a given TOF error $\Delta\mathbf{x}$, the control objective of driving $\mathbf{x}_1$ to $\boldsymbol{A}\,\mathbf{x}_0^*$ can be achieved approximately by selecting $\Delta\mathbf{u}$ such that:

$$\boldsymbol{J}_u\,\Delta\mathbf{u} = -\boldsymbol{J}_x\,\Delta\mathbf{x}\,. \tag{18}$$

Numerical experiments have shown $\boldsymbol{J}_u \in \mathbb{R}^{3\times4}$ to be full rank, which provides redundancy to meet condition (18). To account for this redundancy, the change in spring constant Δk_{s_1} is chosen to be opposite that of Δk_{s_2}. Under this additional constraint, given a $\Delta\mathbf{x}$, there is a unique solution for $\Delta\mathbf{u}$ in (18), with the resulting control law given as:

$$\mathbf{u}_0 = \mathbf{u}_0^* + \boldsymbol{K}(\mathbf{x}_0 - \mathbf{x}_0^*). \tag{19}$$

Similar to arguments in [14], the implicit function theorem can be applied to show that (19) is in fact a first-order approximation to a deadbeat controller that employs $\Delta k_{s_1} = -\Delta k_{s_2}$. The value of $\boldsymbol{K}$ to stabilize periodic running at 3.5 m/s is shown in (20) and displays many expected relationships. For instance, the second column shows which control actions should be taken if the system needs to change forward speed. A positive Δv_x indicates that the system is moving too fast, which requires a larger touchdown angle θ and removal of spring energy $\Delta k_{s_2} < 0$ to correct the error. Similar expected relationships mainly modify ϕ to correct for lateral velocity error. Note that these gains are not tuned, but rather are provided automatically from solution of (18).

$$\begin{bmatrix} \Delta\theta \\ \Delta\phi \\ \Delta k_{s_1} \\ \Delta k_{s_2} \end{bmatrix} = \begin{bmatrix} -0.51 & 0.13 & 0.013 \\ -1.95 & -0.076 & -0.900 \\ 36.9 & 13.2 & -0.86 \\ -36.9 & -13.2 & 0.86 \end{bmatrix} \begin{bmatrix} \Delta h \\ \Delta v_x \\ \Delta v_y \end{bmatrix} \tag{20}$$

Here all angles are measured in radians, distances are measured in meters, and spring constants have units kN/m. Separate feedback matrices $\boldsymbol{K}$ are computed for each of the 31 periodic 3D-SLIP state-control pairs $(\mathbf{x}_0^*, \mathbf{u}_0^*)$, generated in Sec II-C, for speeds from 3.5-6.5 m/s.

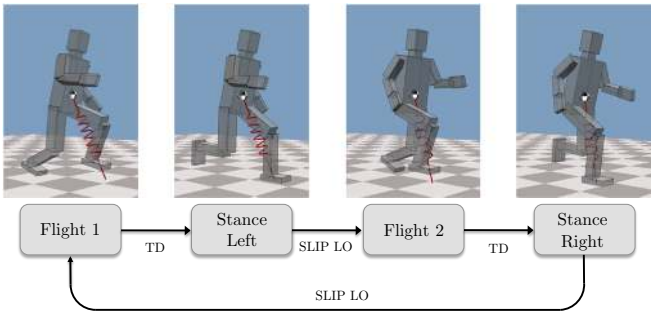

Fig. 5. State machine used for running control. State transition criteria are noted on the transition arrows. Local SLIP deadbeat control occurs at each liftoff to select touchdown angles and target CoM compliance characteristics for the upcoming step.

III. Humanoid Model and Control

A. Humanoid Model

The humanoid model used in this work, shown in Fig. 1, is a 26 degree of freedom (DoF) model, with 20 actuated DoFs. It is modeled after a 6 foot, 160 pound male. The mass distribution to each segment is modeled after a 50-th percentile male, with further details on the relative dimensions and weight distribution provided in [15]. See [15] for a description of the 3D dynamic simulation environment used here. The configuration of the system can be described by $\boldsymbol{q} = [\ \boldsymbol{q}_b^T\ \ \boldsymbol{q}_a^T\ ]^T$, where $\boldsymbol{q}_b \in SE(3)$ is the unactuated position and orientation of the torso (referred to as the floating base) and $\boldsymbol{q}_a$ denotes the configuration of the actuated joints. The joint rate and acceleration vectors, $\dot{\boldsymbol{q}} \in \mathbb{R}^{26}$ and $\ddot{\boldsymbol{q}} \in \mathbb{R}^{26}$, are partitioned similarly. The standard dynamic equations of motion are:

$$\boldsymbol{H}(\boldsymbol{q})\ddot{\boldsymbol{q}} + \boldsymbol{C}(\boldsymbol{q},\dot{\boldsymbol{q}})\dot{\boldsymbol{q}} + \boldsymbol{G}(\boldsymbol{q}) = \boldsymbol{S}_a^T\boldsymbol{\tau} + \boldsymbol{J}_s(\boldsymbol{q})^T\boldsymbol{F}_s \tag{21}$$

where $\boldsymbol{H}$, $\boldsymbol{C}\dot{\boldsymbol{q}}$, and $\boldsymbol{G}$ are the familiar mass matrix, velocity product terms, and gravitational terms, respectively. Here $\boldsymbol{F}_s$ collects ground reaction forces (GRFs) for appendages in support, and $\boldsymbol{J}_s$ is a combined support Jacobian. The matrix $\boldsymbol{S}_a = [\,\mathbf{0}_{20\times6}\ \ \mathbf{1}_{20\times20}\,]$ is a selection matrix for the actuated joints and $\boldsymbol{\tau} \in \mathbb{R}^{20}$ is the joint torque vector. The control approach detailed in the following subsections embeds the 3D-SLIP dynamics into the full dynamics (21) of the humanoid through the use of task-space control. A state machine is used to control the phasing of leg trajectories synchronously with the 3D-SLIP template behavior.

B. State Machine and Commanded Task Dynamics

A running state machine, shown in Fig. 5, is used to to sequence the humanoid through phases of stance and flight. The state machine is assumed to have access to the system state ($\boldsymbol{q}$, $\dot{\boldsymbol{q}}$) in order to formulate desired task dynamics for the feet and CoM to track the 3D-SLIP template behavior. In addition, centroidal angular momentum control is applied in stance due to its postulated role in the maintenance of balance [18], and a pose controller is applied to enable the specification of a desired system configuration. The commanded task dynamics are similar to our previous application

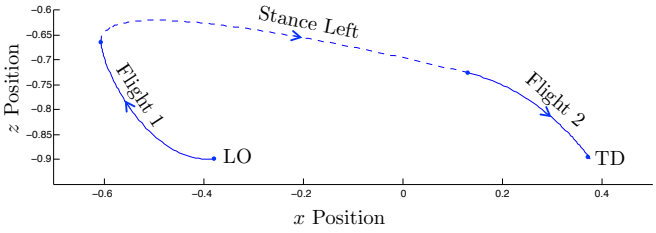

Fig. 6. Right foot trajectory relative to the CoM for running at 3.5 m/s.

of task-space control for a dynamic kick and jump [15]. The task-space controller, described in Section III-C, weighs the commanded task dynamics, which are often in conflict with one another, to select appropriate whole-body joint torques based on task importance through the use of convex optimization.

A foot controller operates in all states to command angular and linear foot accelerations, $\dot{\boldsymbol{\omega}}_c$ and $\ddot{\boldsymbol{p}}_c$, for foot trajectory tracking. For stance feet, this command is set to zero. When the foot is in the air, these rates are selected based on a position/orientation PD scheme [15] with the position PD occurring relative to the CoM:

$$\dot{\boldsymbol{\omega}}_c = \dot{\boldsymbol{\omega}}_d + \boldsymbol{K}_{D,\omega}(\boldsymbol{\omega}_d - \boldsymbol{\omega}) + \boldsymbol{K}_{P,\omega}\boldsymbol{e}_\theta \tag{22}$$

$$\ddot{\boldsymbol{p}}_c = \ddot{\boldsymbol{p}}_d + \boldsymbol{K}_{D,p}(\dot{\boldsymbol{p}}_d - \dot{\boldsymbol{p}}) + \boldsymbol{K}_{P,p}(\boldsymbol{p}_d - \boldsymbol{p}) \ . \tag{23}$$

Here $\boldsymbol{e}_\theta \in \mathbb{R}^3$ is an angle-axis representation of error between a desired and actual orientation.

A simple concatenation of three cubic spline trajectories relative to the CoM is used to provide $(\boldsymbol{p}_d, \dot{\boldsymbol{p}}_d, \ddot{\boldsymbol{p}}_d)$. A sample flight foot trajectory relative to the CoM is shown in Fig. 6. These three cubic splines serve to lift, transfer, and plant the foot. Transfer and touchdown targets are adjusted online based on the SLIP template touchdown angles. Estimated stance and flight times from the SLIP model are used to set the timing of these trajectories. Desired orientations for each foot follow cubic splines on the pitch angle of the foot. Foot pitch angle waypoints are manually specified and do not vary with speed. We note that the foot trajectories end with zero velocity relative to the CoM, which induces losses at impact. Early leg retraction [19] could be added to improve touchdown in future work.

A Centroidal Momentum [18] controller operates in the stance states and commands rates of change in system linear and angular momentum to track the 3D-SLIP trajectories and promote balance. A rate of change in total system linear momentum $\dot{\boldsymbol{l}}_G$ is commanded from PD control of the humanoid CoM (G) to the 3D-SLIP model:

$$\dot{\boldsymbol{l}}_{G,c} = m[\ddot{\boldsymbol{p}}_s + \boldsymbol{K}_{D,\ell}(\dot{\boldsymbol{p}}_s - \dot{\boldsymbol{p}}_G) + \boldsymbol{K}_{P,\ell}(\boldsymbol{p}_s - \boldsymbol{p}_G)] \tag{24}$$

where $\boldsymbol{p}_G$ is the CoM position and m is the total mass of the system. At each LO, the state of the 3D-SLIP template is reset to coincide with that of the humanoid. The apex state $\mathbf{x}$ is predicted, and the 3D-SLIP control law (19) is applied. This control provides target touchdown angles for the upcoming stance to realize a desired speed. The 3D-SLIP model is integrated forward by the state machine in software to provide continuous target dynamics to the humanoid.

The commanded rate of change in centroidal angular momentum $\dot{\boldsymbol{k}}_{G,c}$ takes a simpler form:

$$\dot{\boldsymbol{k}}_{G,c} = -\boldsymbol{K}_{D,k}\boldsymbol{k}_G \ . \tag{25}$$

This law provides a dampening of any excess angular momentum. While the roll and yaw angular momentum are well regulated near zero in human running [20], the pitch angular momentum is not due to leg cycling. With this in mind, pitch angular momentum is ignored by the task-space controller that processes this command.

To achieve pose control, joint accelerations are commanded for actuated joints and the torso orientation. For all examples, this command takes the form of a PD law to a desired pose. For all joints except the shoulder, the desired pose is fixed and has zero rate. For revolute joints:

$$\ddot{q}_{i,c} = \ddot{q}_{i,d} + K_{D,i}(\dot{q}_{i,d} - \dot{q}_i) + K_{P,i}(q_{i,d} - q_i), \tag{26}$$

where $\dot{q}_{i,d} = \ddot{q}_{i,d} = 0$ in all the examples here. For spherical joints and torso orientation, the law (22) is employed. Desired shoulder pitch angles and rates are commanded proportional to those of the opposite virtual leg. This promotes a swinging of the arm in phase with the opposite leg. This angular momentum canceling motion is further modified by the task-space controller which attempts to regulate the yaw angular momentum to zero.

C. Prioritized Task-Space Control

The prioritized task-space control (PTSC) approach presented in [15] is used to select system torques $\boldsymbol{\tau}$ to track the commanded task dynamics. Basically, the approach in [15] produces joint torques $\boldsymbol{\tau}$, contact forces $\boldsymbol{F}_s$, and joint accelerations $\ddot{\boldsymbol{q}}$ that are consistent with the dynamic equations of motion in order track the commanded task dynamics:

$$\min_{\ddot{\boldsymbol{q}},\boldsymbol{\tau},\boldsymbol{F}_s} \quad \frac{1}{2}||\boldsymbol{A}_t\,\ddot{\boldsymbol{q}} + \dot{\boldsymbol{A}}_t\,\dot{\boldsymbol{q}} - \dot{\boldsymbol{r}}_{t,c}||^2 \tag{27}$$

$$\text{subject to } \boldsymbol{H}\,\ddot{\boldsymbol{q}} + \boldsymbol{C}\,\dot{\boldsymbol{q}} + \boldsymbol{G} = \boldsymbol{S}_a^T\boldsymbol{\tau} + \boldsymbol{J}_s(\boldsymbol{q})^T\boldsymbol{F}_s \tag{28}$$

$$\boldsymbol{F}_s \in \boldsymbol{\mathcal{C}} \tag{29}$$

Here $\dot{\boldsymbol{r}}_{t,c}$ collects all the commanded task dynamics, while $\boldsymbol{A}_t$ can be viewed as a task Jacobian [15]. The ground reaction force constraint (29) collects unidirectional and friction constraints, with further details in [15]. This optimization can be run multiple times if a strict task hierarchy exists.

For all running results, the foot positions and orientations are set as a first priority, with all other tasks as a secondary priority. Task weightings can be incorporated into the error norm (27) to encourage better tracking of certain tasks. Here, arm task weightings are reduced to provide upper-body motion freedom to the task-space controller. Task weightings and gains are summarized in Table I, with further details on the construction of $\dot{\boldsymbol{r}}_{t,c}$ provided in [15]. Precise tuning of these values is not required to produce stable running, but does affect the nuances of the motion due to task tradeoffs. The task-space control optimization problem (27)-(29) is able to be solved at real-time rates of 200 Hz [15].

Task	Weight	K_P (s^{-2})
CoM	25	150
Angular Momentum	(20,4,20)	$K_D = 25$ s^{-1}
Torso Orientation	(17.5, 70, 14)	440
Hip	0.1	120
Knee	0.5	120
Ankle	0.1	120
Shoulder	17	280
Elbow	20	240
Foot Position & Orientation	1	50

TABLE I

WEIGHT AND GAIN SETTINGS FOR THE PTSC. WHERE OMITTED, ALL DERIVATIVE GAINS ARE SET FOR CRITICAL DAMPING.

IV. RESULTS

The use of a high-level 3D-SLIP controller coupled with a lower-level task-space controller is shown to enable high-speed humanoid running that is able to change speeds and recover from disturbances. This section presents running results at a fixed speed and then demonstrates the tracking capabilities of the controller. The same commanded task gains, task-space weightings, and task-space priorities are employed across all results.

A. Steady-State Fixed-Speed Running

The capabilities of the controller are shown for running at a commanded speed of 3.5 m/s. For a video of the running motion, please see the attachment to this paper, or view it at the link below.

`http://www.go.osu.edu/Wensing_Orin_IROS2013`

The CoM velocity tracking of the task-space controller is shown in Fig. 7. Despite the impact at TD, the controller is able to provide tracking of the CoM velocity to that of the SLIP model in all directions. This impulse, not captured in the 3D-SLIP model, represents a disturbance that is effectively handled by the PTSC. Note that the CoM tracking is not given explicit priority over other commanded task dynamics such as torso orientation or angular momentum. Although explicit CoM prioritization does lead to better tracking results for the CoM, it was found that the system is more robust to disturbances when CoM tracking is not prioritized. Still, the error in TOF forward velocity is approximately 2% for the results in the graph shown.

The angular momentum control applied has advantages to prevent the feet from slipping due to excess required yaw moments. Figure 8 shows the contribution of the upper and lower body to the overall centroidal yaw angular momentum. The task-space controller results in upper-body motions that cancel the majority of the yaw angular momentum of the lower body. This role of the arms in the regulation of yaw angular momentum is a characteristic that is observed in human running [20]. Note that the derivative (slope) of the total yaw angular momentum curve is equal to the generated yaw moment at the foot. The application of yaw momentum control coupled with the arm swing heuristic has effectively decreased the required yaw moment at the feet during stance.

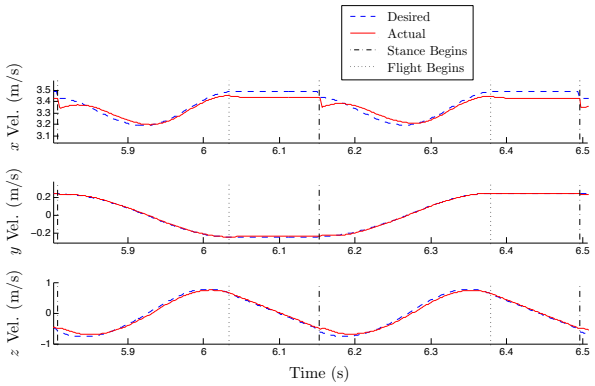

Fig. 7. CoM velocity tracking for running at a desired speed of 3.5 m/s. The velocities in the forward (x) and vertical (z) directions are 1-step periodic, while the lateral velocity (y) is 2-step periodic.

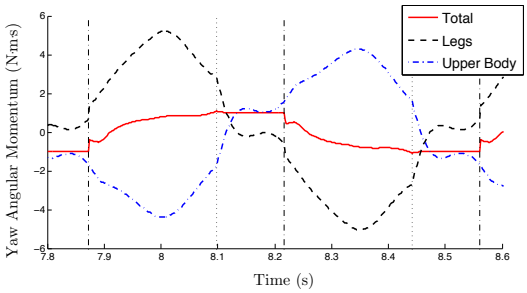

Fig. 8. Yaw angular momentum about the CoM as contributed by the legs and the upper body. The combination of a simple target arm motion and centroidal angular momentum control cause the upper body to cancel the majority of the yaw angular momentum generated by leg cycling.

B. Running Transitions and Push Disturbances

The 3D-SLIP controller provides the task-space controller with reference CoM dynamics to change speeds and recover from push disturbances. Fig. 9 shows the tracking of a commanded forward velocity profile. We note that for each commanded speed, a periodic 3D-SLIP solution (13) and a 3D-SLIP control law (19) have been computed offline. This amounts to storing a small amount of information, $(\mathbf{x}_0, \mathbf{u}_0, \boldsymbol{K})$, for each desired speed. The controller is able to accelerate at up to 0.2 m/s per step and decelerate at up to 0.4 m/s per step. The controller is unable to accelerate faster, as the approximate deadbeat controller does not take into account constraints on the touchdown angle which are required to limit the minimum touchdown angle θ based

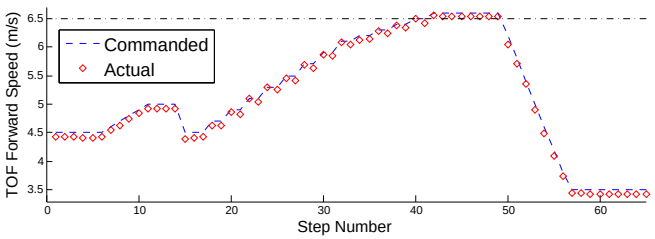

Fig. 9. Tracking of a commanded forward velocity profile. Local deadbeat control of the 3D-SLIP model provides foot placement and target CoM dynamics to enable velocity transitions.

on the TOF height. Once again, the CoM is not explicitly prioritized, which prevents perfect tracking at TOF but improves robustness to disturbances.

Figure 10 shows the response of the system to a series of lateral disturbances. Pushes are either 1000 N or 750 N and are applied for 40 ms. The system is able to maintain balance when the same pushes are applied in the sagittal plane as well. Lateral push recovery is detailed here, as its out-of-plane dynamics are a new complexity that is managed by the 3D-SLIP controller. All pushes occur during stance. For instance, the first push occurs during a right foot stance immediately before liftoff. The 3D-SLIP controller picks touchdown angles that modify the left foot touchdown to reject this additional y velocity. A push to the left can also be rejected with the left foot is in stance, by taking a cross step with the right foot. This is shown in the next series of 3 disturbances (each 30 N·s) that occur in succession. The final two 40 N·s pushes occur earlier in stance, and can be partially rejected by the CoM controller in stance. These require less extreme recovery footsteps, but result in different torso dynamics, as shown in the video attachment. Although steady-state running is largely dominated by sagittal plane dynamics, these out-of-plane disturbance recovery results are unable to be described by planar SLIP models. This result showcases a major advantage of applying the 3D-SLIP.

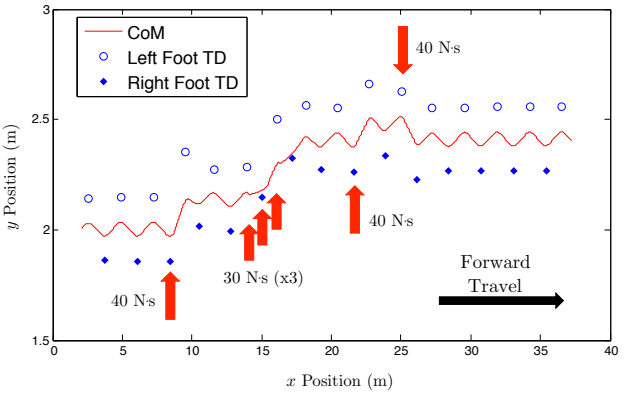

Fig. 10. Footstep selection for lateral disturbance rejection. Shown are the actual touchdown locations of the humanoid foot. Target footsteps are selected from local deadbeat control of the 3D-SLIP model.

V. Conclusion

This paper has presented a control approach for high-speed running in a simulated humanoid robot. Local deadbeat control applied to a 3D-SLIP template model provides appropriate dynamics online for the system to change speeds and recover from large disturbances. While the local deadbeat control is only approximate, the simple form of the control law enables use online. When coupled with a task-space controller that operates at real-time rates, these corrective reference CoM dynamics are accurately reproduced by the simulated humanoid. To the best of the authors' knowledge, these results represent the first application of the 3D-SLIP model to the control of a whole-body humanoid system. These positive results encourage the use of low-complexity template models to control and study balance for other high-speed movements. As parallel advances continue to develop improved inertial sensing technologies and increased torque/speed capacity actuators, these dynamic behaviors may soon be within reach for humanoid robots.

VI. Acknowledgments

This work was supported by a National Science Foundation Graduate Research Fellowship to Patrick Wensing, and by Grant No. CNS-0960061 from the NSF with a subaward to The Ohio State University.

References

[1] R. Blickhan and R. Full, "Similarity in multilegged locomotion: Bouncing like a monopode," *Journal of Comparative Physiology A*, vol. 173, pp. 509–517, 1993.

[2] D. P. Ferris, M. Louie, and C. T. Farley, "Running in the real world: adjusting leg stiffness for different surfaces," *Proceedings of the Royal Society of London. Series B: Biological Sciences*, vol. 265, no. 1400, pp. 989–994, 1998.

[3] D. F. Hoyt and C. R. Taylor, "Gait and the energetics of locomotion in horses," *Nature*, vol. 292, pp. 239–240, July 1981.

[4] J. Hurst and A. Rizzi, "Series compliance for an efficient running gait," *IEEE Rob. Auto. Magazine*, vol. 15, pp. 42–51, Sept. 2008.

[5] S. Kajita, T. Nagasaki, K. Kaneko, and H. Hirukawa, "ZMP-based biped running control," *IEEE Robotics and Automation Magazine*, vol. 14, pp. 63–72, June 2007.

[6] T. Takenaka, T. Matsumoto, T. Yoshiike, and S. Shirokura, "Real time motion generation and control for biped robot -2nd report: Running gait pattern generation-," in *IEEE/RSJ Int. Conf. on Intelligent Robots and Systems*, pp. 1092–1099, Oct. 2009.

[7] J. Hodgins, "Three-dimensional human running," in *IEEE Int. Conf. on Rob. and Automation*, vol. 4, pp. 3271–3276, Apr. 1996.

[8] T. Erez and E. Todorov, "Trajectory optimization for domains with contacts using inverse dynamics," in *IEEE/RSJ International Conference on Intelligent Robots and Systems*, pp. 4914–4919, Oct. 2012.

[9] I. Poulakakis and J. Grizzle, "The spring loaded inverted pendulum as the hybrid zero dynamics of an asymmetric hopper," *IEEE Transactions on Automatic Control*, vol. 54, pp. 1779–1793, Aug. 2009.

[10] M. Hutter, C. Remy, M. Hopflinger, and R. Siegwart, "SLIP running with an articulated robotic leg," in *IEEE/RSJ Int. Conf. on Intelligent Robots and Systems*, pp. 4934–4939, Oct. 2010.

[11] M. Rutschmann, B. Satzinger, M. Byl, and K. Byl, "Nonlinear model predictive control for rough-terrain robot hopping," in *IEEE/RSJ Int. Conf. on Intelligent Robots and Systems*, pp. 1859–1864, Oct. 2012.

[12] G. Garofalo, C. Ott, and A. Albu-Schaffer, "Walking control of fully actuated robots based on the bipedal SLIP model," in *IEEE Int. Conf. on Robotics and Automation*, pp. 1456–1463, May 2012.

[13] J. E. Seipel and P. Holmes, "Running in three dimensions: Analysis of a point-mass sprung-leg model," *The International Journal of Robotics Research*, vol. 24, no. 8, pp. 657–674, 2005.

[14] S. Carver, *Control of a Spring Mass Hopper*. PhD thesis, Cornell University, Ithaca, NY, 2003.

[15] P. M. Wensing and D. E. Orin, "Generation of dynamic humanoid behaviors through task-space control with conic optimization," in *IEEE Int. Conf. on Rob. and Automation*, pp. 3088–3094, May 2013.

[16] A. Rowlands, M. Stone, and R. Eston, "Influence of speed and step frequency during walking and running on motion sensor output," *Med. & Science in Sports & Exercise*, vol. 39, no. 4, pp. 716–727, 2007.

[17] D. Hoyt, S. Wickler, and E. Cogger, "Time of contact and step length: the effect of limb length, running speed, load carrying and incline," *Journal of Experimental Biology*, vol. 203, no. 2, pp. 221–227, 2000.

[18] D. E. Orin and A. Goswami, "Centroidal momentum matrix of a humanoid robot: Structure and properties," in *IEEE/RSJ Int. Conf. on Intelligent Robots and Systems*, (Nice, France), pp. 653–659, Sept. 2008.

[19] L. Palmer and D. Orin, "Quadrupedal running at high speed over uneven terrain," in *IEEE/RSJ Int. Conf. on Intelligent Robots and Systems*, pp. 303–308, Nov. 2007.

[20] R. N. Hinrichs, "Upper extremity function in running. II: Angular momentum considerations," *International Journal of Sport Biomechanics*, vol. 3, no. 3, pp. 242–263, 1987.